A Multiple Radioactive Particle Tracking Technique to Investigate Particulate Flows

Majid Rasouli, Francois Bertrand, and Jamal Chaouki
Dept. of Chemical Engineering, École Polytechnique de Montréal, C.P. 6079, Succursale Centre-Ville, Montréal, QC, Canada H3C 3A7

DOI 10.1002/aic.14644
Published online October 16, 2014 in Wiley Online Library (wileyonlinelibrary.com)

Radioactive particle tracking is a nonintrusive technique that has been successfully used to study the flow dynamics in a wide range of reactors and blenders. However, it is still limited to the tracking of only one tracer at a time. A multiple radioactive particle tracking (MRPT) technique that can determine the trajectory of two free or restricted (attached to the same particle) moving tracers in a system is introduced. The accuracy (<5 mm) and precision (<5 mm) of the proposed technique is evaluated by tracking two stationary tracers and two moving tracers. The results confirm the reliability and validity of the MRPT technique when the two tracers have the same isotope and the distance between them is not too small (>2 cm). The tracking of two sticking tracers at the two ends of a cylindrical particle in a rotating drum is also considered to illustrate the potential of this characterization method. © 2014 American Institute of Chemical Engineers *AIChE J*, 61: 384–394, 2015

Keywords: radioactive particle tracking, solid mixing, rotating drum, cylindrical particle, nonspherical particle

Introduction

In chemical engineering, reliable measurement of the flow dynamics in various systems is essential. To do so, sophisticated measuring techniques have been developed and improved by advances in computer control and instrumentation technology.[1] These improvements are of two types, namely the reduction of the measurement volume and the degree of intrusiveness, and have lead to two different categories of measurement techniques. The first category, which provides locally refined information about the flow structure, is composed, for instance, of capacitance and fiber-optic probes.[2] The second category is characterized by the absence of side effects coming from the interaction between the medium and the measurement apparatus[2]; it includes optical techniques such as laser Doppler anemometry and particle image velocimetry, and radioactive techniques such as radioactive particle tracking (RPT)[2] and positron emission particle tracking (PEPT).[3] The optical methods are essentially limited to transparent systems while radioactive techniques can be applied in opaque systems, because gamma rays can penetrate relatively easily through various materials. PEPT uses two positron-sensitive detectors mounted on the opposite sides of a system to detect pairs of exactly back to back gamma rays resulting from the annihilation of a positron.[3–8] This technique is able to detect a tracer when this tracer is within the volume covered by the detectors. RPT uses an array of several compact sodium iodide (NaI-Tl) detectors, which can be flexibly arranged around the system. As RPT and PEPT use different detectors and rely on different algorithms to reconstruct tracer trajectories, they have their own advantages and drawbacks. For instance, RPT setups are compact, flexible, and cheap compared to those of PEPT.[9] Conversely, it is not trivial to extend RPT to systems with irregular moving boundaries.[9]

RPT was developed by Lin et al.[10] in 1980s to track the motion of a single particle noninvasively in fluidized beds. In this method, a labeled tracer particle, a data acquisition system and a location algorithm are used to calculate the tracer position, as illustrated in Figure 1 in the case of granular flow in a rotating drum. The tracer is a labeled particle containing an irradiated radionuclide, such as ^{46}Sc and ^{24}Na,[11,12] which decays due to the emission of gamma rays. The data acquisition system, which consists of an array of sodium iodide (NaI-Tl) detectors, amplifier/discriminators, and high-speed counters, records the number of gamma rays—the so-called event counts—coming from the tracer, which are almost completely absorbed inside the detectors during the sampling time. The location algorithm will be described in detail in the following section. Several publications, principally by the groups of Chaouki and Dudukovic, on the application of RPT for gas, liquid, and three-phase fluidized beds,[13–17] bubble columns,[18,19] stirred tanks,[20,21] spouted beds,[22,23] V-blender,[9,24] and rotating drums[25–27] have showed the capabilities of this technique for monitoring the flow dynamics in various systems. A few investigations to improve the accuracy of RPT results by choosing a proper radionuclide for the tracer,[11,12] designing an optimal setup with respect to the sensitivity of the detectors,[12] and removing saturated detectors from location calculations,[28] have also been reported. In addition, RPT has been modified to visualize the tracer motion online,[11] and extended to systems

Correspondence concerning this article should be addressed to F. Bertrand at francois.bertrand@polymtl.ca or J. Chaouki at jamal.chaouki@polymtl.ca.

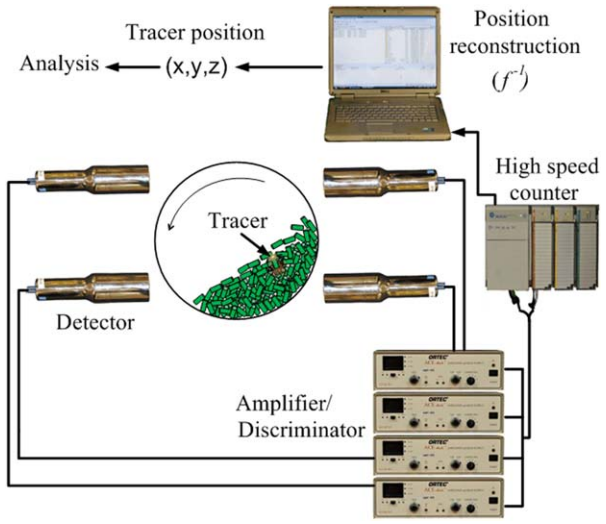

Figure 1. Typical RPT setup for a rotating drum.

[Color figure can be viewed in the online issue, which is available at wileyonlinelibrary.com.]

with irregular moving boundaries[9] as well as systems with high velocities.[28]

Although RPT has showed powerful noninvasive tracking abilities in different processes, it is still limited to the tracking of only one tracer at a time. Tracking more than one particle simultaneously is definitely of interest because it could yield direct information about both the translational and rotational motions of particles. In particular, the rotational motion of particles may play a significant role for instance on the lift force exerted on them and then have an impact on their distribution.[29] In systems where heat transfer is involved, the rotational motion of solid particles may change the rate of heating or cooling by increasing the interphase heat transfer coefficient.[30,31] In addition, by tracking more than one particle at the same time, the effect of the spatial orientation of nonspherical particles when they hit the wall of a system or bubbles in a fluidized bed, as well as the relative motion of two freely moving particles, can be studied. Furthermore, the validation of discrete element-based models is another reason why the tracking of multiple particles is of interest.

In this study, a so-called multiple radioactive particle tracking (MRPT) technique that is capable of simultaneously tracking two tracers, which can move freely or are constrained to stay at a fixed distance from each other, is introduced. This method will be first explained in detail, followed by two types of experiments to show its potential. It will then be applied to a rotating drum filled with cylindrical particles mixed with spherical glass beads.

Method

RPT location algorithm

The RPT location algorithm calculates the spatial position of the tracer ($\boldsymbol{X}=(x,y,z)$) from the set of event counts ($\Phi=\{\Phi_i\}_{i=1..N}$) recorded by the data acquisition system (each of the N detectors). The latest generation of this algorithm is based on a phenomenological model that predicts the event counts for each detector for given tracer positions.[9,32,33] As there is no analytical inverse function for this model, the algorithm uses a direct search method and seeks the tracer position corresponding to a given set of event counts by covering the entire domain of the system. To do so, the algorithm relies on a discretization of the domain into tetrahedra and nodes, and calculates a set of event counts for the detectors corresponding to each of these nodes. The algorithm then reconstructs the tracer position by solving a minimization problem that yields the smallest gap between the measured and calculated sets of event counts. The phenomenological model and minimization procedure will be presented and discussed in the next two sections, followed by the introduction of the MRPT technique.

Phenomenological model

For a given system, the number of detected gamma rays (event counts) recorded by a detector is function of the relative position of the tracer and the material between this detector and this tracer. This relationship can be approximated by a phenomenological model that relates the number of events for detector j to the position of the tracer[34,35]

$$\Phi_j(\boldsymbol{X})=\frac{T\upsilon R\phi\xi_j(\boldsymbol{X},\mu_s)}{1+\tau\upsilon R\phi\xi_j(\boldsymbol{X},\mu_s)} \tag{1}$$

where T is the sampling time, υ is the number of photons emitted by disintegration ($\upsilon=2$ for ^{46}Sc),[15] R is the tracer activity, ϕ is the photopeak-to-total ratio ($\phi=0.40$ for ^{46}Sc),[15] τ is the dead time of the acquisition system, and $\Phi_j(\boldsymbol{X})$ and $\xi_j(\boldsymbol{X},\mu_s)$ represent the event counts and the efficiency of detector j with respect to position $\boldsymbol{X}$, respectively. In Eq. 1, the efficiency term $\xi_j(\boldsymbol{X},\mu_s)$, which brings into play the attenuation coefficient μ_s, is the only variable that depends on the tracer position and the most challenging term to evaluate. By definition, the efficiency is the fraction of emitted gamma rays that hit a given detector as they travel across the system.[36] As there is no analytical solution for this efficiency, except in some simple cases, a Monte Carlo technique has been devised to compute it.[9,15,32,33,35]

Reconstruction of the tracer position

To minimize scattering and back-reflection effects, gamma rays outside of a certain energy window are rejected using an amplifier/discriminator. To take into account the amplification and discrimination of the original pulses during the data acquisition process, and to obtain the attenuation coefficient of the system μ_s, a calibration test is performed prior to each RPT experiment. The tracer is positioned in n given positions $\{\boldsymbol{X}_k\}_{k=1..n}$ inside of the system. For each detector j, the attenuation coefficient of the system μ_s, the tracer activity R, and the dead time of the acquisition system τ are fitted by solving the minimization problem

$$\min_{R,\tau,\mu_s}\sum_{k=1}^{n}\left(\frac{\Phi_j(\boldsymbol{X}_k)-\Phi_j^m}{\Phi_j(\boldsymbol{X}_k)+\Phi_j^m}\right)^2 \tag{2}$$

where $\Phi_j(\boldsymbol{X}_k)$ and Φ_j^m are the calculated and measured event counts for detector j with respect to position $\boldsymbol{X}_k$, respectively.

As the calculation of event counts is time consuming, the algorithm saves them in a matrix, the so-called dictionary, so that this information is readily available when needed. More precisely, for each detector, a dictionary is built, which contains the calculated event counts associated with all the nodes used to discretize the domain of the system V (see Dube et al.[37] for the nodal geometry). Then, for a given set

of measured event counts, the algorithm seeks the node P_i yielding the smallest gap between the corresponding set of calculated event counts and these measured event counts by solving

$$\min_{P_i \in V} \sum_{j=1}^{N} \left(\frac{\Phi_j(P_i) - \Phi_j^m}{\Phi_j(P_i) + \Phi_j^m} \right)^2 \tag{3}$$

After obtaining node P_i, the algorithm further refines the position of tracer $\boldsymbol{X}_P$ by searching every tetrahedron T_P that contains this node

$$\min_{X_P \in T_P} \sum_{j=1}^{N} \left(\frac{\Phi_j(\boldsymbol{X}_P) - \Phi_j^m}{\Phi_j(\boldsymbol{X}_P) + \Phi_j^m} \right)^2 \tag{4}$$

A linear interpolation is used to compute the values of the event counts at $\boldsymbol{X}_P$ based on the values at the nodes of the corresponding tetrahedron.

MRPT technique

When adding a second tracer, the data acquisition system records the event counts resulting from both tracers. As the contribution of each of these tracers on the recorded event counts is not known, the location algorithm cannot be applied in a straightforward manner. To get around this problem, two approaches may be considered: (a) determine the contribution of each tracer on the recorded event counts or (b) create a new location algorithm that can deal with the combined recorded event counts.

In the first approach, the tracers should be built from two different isotopes, where one has a high gamma energy peak significantly different from the other energy peaks. The amplifiers/discriminators of the acquisition system can be divided into two groups. The first group only captures gamma rays that have energies within a range around the highest energy peak. The second group records gamma rays that have energies within a window covering the other energy peaks. Consequently, one possibility would consist of positioning the highest energy peak tracer (made from one of the two isotopes) using the current RPT algorithm. The phenomenological model presented in the previous section could then serve to calculate the tracer position, and the contribution of this first tracer on the events recorded by the second group of amplifiers/discriminators could be calculated and subtracted from the total event counts monitored by this group. This would enable the positioning of the second tracer with the current RPT algorithm. However, it is known that some of the gamma rays with the highest energy peak scatter when they interact (Compton scattering or pair production) so that they lose energy and end up within the range of the other energy window. Therefore, these gamma rays are recorded by the second group of amplifiers/discriminators and their contribution is not subtracted from the recorded event counts. The number of such gamma rays varies depending on their travel distance and the material that they pass through, as well as on the random nature of the radioactive interactions (further discussion is provided in Appendix). These gamma rays represent noise for the second tracer, which increases the noise to signal ratio and leads to poor positioning. This method is then difficult to use in practice.

In the other approach, the second tracer (tracer B) is built with the same isotope as the first tracer (tracer A). Therefore, the data acquisition system records the event counts resulting from both tracers. As the contribution of each tracer on the collected event counts is not known, the standard RPT location algorithm is not applicable. To overcome this problem, it is proposed to seek the position of the two tracers simultaneously instead of tracking each tracer individually. Consequently, the algorithm must be adapted to handle this new tracking technique. More precisely, it should be able to predict event counts resulting from two tracers located at two given positions. In fact, because of the dead time of the acquisition system, the superposition property does not hold for the measured event counts.[34,36] However, this property is still correct for the actual event count rate associated to detector j

$$N_j^{(\mathrm{A,B})}(\boldsymbol{X}_\mathrm{A}, \boldsymbol{X}_\mathrm{B}) = N_j^\mathrm{A}(\boldsymbol{X}_\mathrm{A}) + N_j^\mathrm{B}(\boldsymbol{X}_\mathrm{B}) \tag{5}$$

where $N_j^{(\mathrm{A,B})}(\boldsymbol{X}_\mathrm{A}, \boldsymbol{X}_\mathrm{B})$ is the actual event count rate resulting from both tracers A and B at positions $\boldsymbol{X}_\mathrm{A}$ and $\boldsymbol{X}_\mathrm{B}$, with respect to detector j. $N_j^\mathrm{A}(\boldsymbol{X}_\mathrm{A})$ and $N_j^\mathrm{B}(\boldsymbol{X}_\mathrm{B})$ are the actual event count rates for tracers A and B at position $\boldsymbol{X}_\mathrm{A}$ and $\boldsymbol{X}_\mathrm{B}$, with respect to detector j.

There is a relationship between the actual event count rate N_j, the measured event counts Φ_j for sampling time T and dead time τ[34,36]

$$N_j^\mathrm{I}(\boldsymbol{X}_\mathrm{I}) = \frac{\left(\Phi_j^\mathrm{I}(\boldsymbol{X}_\mathrm{I})/T\right)}{1 - \tau\left(\Phi_j^\mathrm{I}(\boldsymbol{X}_\mathrm{I})/T\right)}, \quad \mathrm{I} = \mathrm{A,B \text{ or } (A,B)} \tag{6}$$

Substituting (6) into (5) then yields

$$\frac{\left(\Phi_j^{(\mathrm{A,B})}(\boldsymbol{X}_\mathrm{A}, \boldsymbol{X}_\mathrm{B})/T\right)}{1 - \tau\left(\Phi_j^{(\mathrm{A,B})}(\boldsymbol{X}_\mathrm{A}, \boldsymbol{X}_\mathrm{B})/T\right)} = \frac{\left(\Phi_j^\mathrm{A}(\boldsymbol{X}_\mathrm{A})/T\right)}{1 - \tau\left(\Phi_j^\mathrm{A}(\boldsymbol{X}_\mathrm{A})/T\right)} + \frac{\left(\Phi_j^\mathrm{B}(\boldsymbol{X}_\mathrm{B})/T\right)}{1 - \tau\left(\Phi_j^\mathrm{B}(\boldsymbol{X}_\mathrm{B})/T\right)} \tag{7}$$

Rearranging Eq. 7 results in a model that can predict the total measured event counts coming from both tracers based on the individual measured event counts

$$\Phi_j^{(\mathrm{A,B})}(\boldsymbol{X}_\mathrm{A}, \boldsymbol{X}_\mathrm{B}) = \frac{\Phi_j^\mathrm{A}(\boldsymbol{X}_\mathrm{A}) + \Phi_j^\mathrm{B}(\boldsymbol{X}_\mathrm{B}) - 2\left(\tau/T\right)\Phi_j^\mathrm{A}(\boldsymbol{X}_\mathrm{A})\Phi_j^\mathrm{B}(\boldsymbol{X}_\mathrm{B})}{1 - \left(\tau/T\right)^2 \Phi_j^\mathrm{A}(\boldsymbol{X}_\mathrm{A})\Phi_j^\mathrm{B}(\boldsymbol{X}_\mathrm{B})} \tag{8}$$

where $\Phi_j^{(\mathrm{A,B})}(\boldsymbol{X}_\mathrm{A}, \boldsymbol{X}_\mathrm{B})$ is the calculated event count resulting from both tracers A and B at positions $\boldsymbol{X}_\mathrm{A}$ and $\boldsymbol{X}_\mathrm{B}$, with respect to detector j. $\Phi_j^\mathrm{A}(\boldsymbol{X}_\mathrm{A})$ and $\Phi_j^\mathrm{B}(\boldsymbol{X}_\mathrm{B})$ are the event counts calculated from Eq. 1 for tracers A and B at position $\boldsymbol{X}_\mathrm{A}$ and $\boldsymbol{X}_\mathrm{B}$, with respect to detector j.

Prior to a two-radioactive-particle tracking experiment, two calibration tests are first performed to obtain the fitted parameters of Eq. 1 for tracers A and B, individually. Using a procedure similar to that for the RPT algorithm, dictionaries are built for each tracer with respect to each detector. For a given set of measured event counts, the algorithm then seeks the nodes P_i for the tracer A and P_k for the tracer B yielding the smallest gap between the sets of calculated and measured event counts by solving

$$\min_{P_i, P_k \in V} \sum_{j=1}^{N} \left(\frac{\Phi_j^{(A,B)}(P_i, P_k) - \Phi_j^m}{\Phi_j^{(A,B)}(P_i, P_k) + \Phi_j^m} \right)^2 \tag{9}$$

After obtaining the pair of nodes P_i and P_k, the algorithm further refines the positions of tracers $\boldsymbol{X}_\mathrm{A}$ and $\boldsymbol{X}_\mathrm{B}$ by

searching tetrahedra T_{P_i} and T_{P_k} that contain nodes P_i and P_k, respectively

$$\min_{\substack{X_A \in T_{P_i} \\ X_B \in T_{P_k}}} \sum_{j=1}^{N} \left(\frac{\Phi_j^{(A,B)}(X_A, X_B) - \Phi_j^m}{\Phi_j^{(A,B)}(X_A, X_B) + \Phi_j^m} \right)^2 \quad (10)$$

A linear interpolation is used to compute the values of the event counts at X_A and X_B based on the values at the nodes of the corresponding tetrahedra.

Experimental

The isotope used for tracers A and B is scandium-46 (^{46}Sc). To choose the activities of the tracers, there were two considerations. First, for the setup used, the summation of the tracer activities should be less than 95 μCi to avoid saturation of the detectors. Second, the tracers should have different activities so that they can be identified. Therefore, activities of 53 and 39 μCi were chosen for tracers A and B, respectively. Twelve 76 × 76 mm^2 NaI (Tl) scintillation detectors (Teledyne Isotope S-1212-I) are positioned around the setup (Figure 2) on two levels in the vertical direction. Each detector is connected to a scintillation tube and the signal is amplified and discriminated by an ORTEC ACE Mate amplifier/discriminator (925-Scint). The sampling time T for the measurements is 10.0 ms, which corresponds to 100 locations per second. In this study, two types of experiments were done: (a) one for the validation of the MRPT technique and (b) one for the application of this new method. These two groups of experiments are the topic of the next two subsections, respectively.

Validation of the MRPT technique

These experiments were conducted in a plexiglass column with a 15 cm diameter and filled with water up to 12 cm in height. They involved: (a) two tracers that can move freely (the so-called free MRPT) or (b) two tracers at a fixed distance from each other (the so-called restricted MRPT). To assess the accuracy and precision of the MRPT technique, these experiments were carried out with stationary and moving tracers for both free and restricted MRPT.

In the stationary particle tests, the accuracy and precision of the MRPT technique were evaluated by reconstructing the tracer positions, the tracers being located at fixed positions. In the case of the free MRPT, the sources were placed at eight different distances from each other. In the case of the restricted MRPT, three rod-like tracers were built by fixing radioactive sources at the two ends of three acrylic rods with a 6 mm diameter and 2, 3, and 4 cm in length, respectively. Each tracer was placed in 12 different positions and six different orientations. Each such stationary particle test was performed for 12 s.

In the moving particle tests, the effect of the tracer speed was assessed on the basis of the quality of the reconstruction of the tracer positions, these tracers having known displacements and speeds (circular motion). To control the displacement of the tracers, an electromotor with a constant rotational speed of 10.5 rpm was vertically installed at the top of the column (see Figure 2). The middle of an adjustable arm was perpendicularly joined to the shaft of the electromotor. Therefore, by fixing the tracers to the arm and

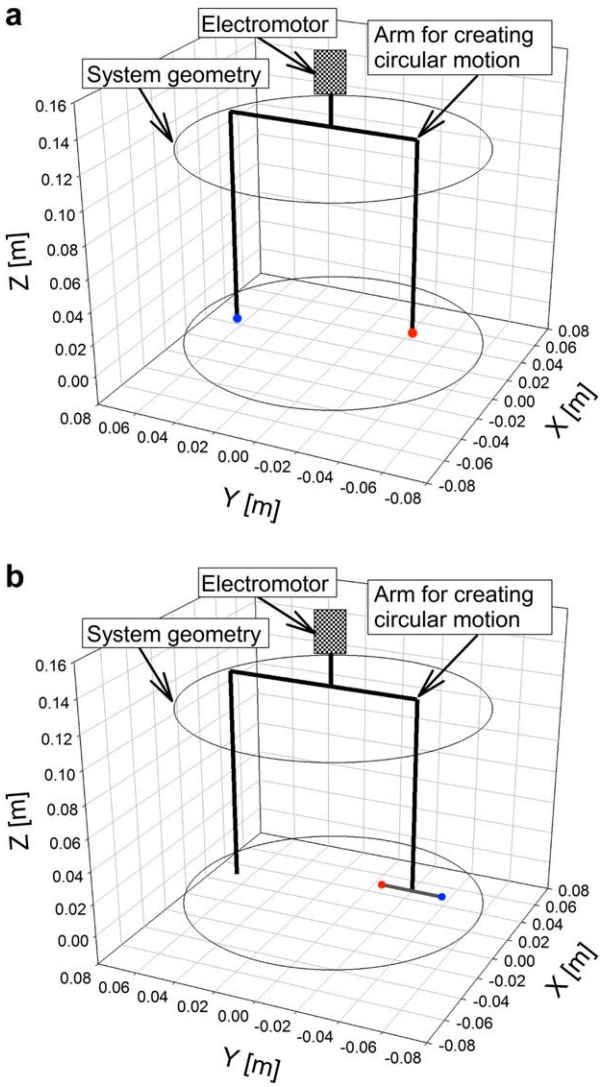

Figure 2. Schematic of the experimental setup for (a) moving free MRPT and (b) moving restricted MRPT test.

[Color figure can be viewed in the online issue, which is available at wileyonlinelibrary.com.]

adjusting the arm length, a circular motion with given radii was generated. In the case of the free MRPT (Figure 2a), two tracers each with its own radius were set in circular motion by attaching the two corresponding sources to the two arm tips. For the restricted MRPT (Figure 2b), each rod-like tracer was set in circular motion by fixing it to one tip of the arm, in such a way that the line going through the two sources is perpendicular to the axis of the shaft of the electromotor. All the moving particle experiments lasted 3 min.

Example of application

This type of experiment was conducted in a rotating drum 24 cm in diameter and 38 cm in length. The drum was filled to 35 vol % with acrylic cylindrical particles (20% v/v) 6 mm in diameter and 3 cm in length, and spherical glass beads (80% v/v) 3 mm in diameter. The drum rotational speed was set at 2.5 rpm. All the particles were uniformly

mixed at the beginning. A rod-like tracer 3 cm in length was used to mimic the motion of the cylindrical particles.

Results and Discussion

Validation tests

The accuracy (degree of closeness of the measurements) of the MRPT technique can be evaluated by comparing the actual and measured average values of the tracer positions (p) and speeds (s) and, in the case of a rod-like tracer, of the orientations (α)

$$px_k = \left| \frac{\sum_{i=1}^{M} \hat{x}_k^i}{M} - x_k \right| \tag{11}$$

$$sx_k = \left| \frac{\sum_{i=1}^{M} \hat{v}x_k^i}{M} - vx_k \right| \tag{12}$$

$$\alpha = \left(\frac{\sum_{i=1}^{M} \mathrm{acos}(\overrightarrow{t_i}.\mathrm{t})}{M} \right) \times 180/\pi \tag{13}$$

The precision (reproducibility) can be assessed through the standard deviation of the measured values of the tracer positions and, in the case of a rod-like tracer, of the orientations

$$\sigma_{xk} = \sqrt{\sum_{i=1}^{M} \left(\hat{x}_k^i - \frac{\sum_{j=1}^{M} \hat{x}_k^j}{M} \right)^2 \Big/ M} \tag{14}$$

$$\sigma_k = \sqrt{\sigma_{xk}^2 + \sigma_{yk}^2 + \sigma_{zk}^2} \tag{15}$$

$$\sigma_\alpha = \sqrt{\sum_{i=1}^{M} \left(\mathrm{acos}(\overrightarrow{t_i}.\overrightarrow{t}) \right)^2 / M} \tag{16}$$

In these expression, x_k represents the actual position of tracer k, px_k and sx_k are the errors of the MRPT results on the position and speed of tracer k along the x axis, respectively, $\hat{x}_k^i$ and $\hat{v}x_k^i$ the ith calculated position and speed of tracer k along the x axis, respectively, $\overrightarrow{t}$ and $\overrightarrow{t_i}$ the actual and the ith calculated value of the unit vector representing the rod-like tracer, respectively, σ_{xk} the standard deviation of the position of tracer k along the x axis, and M the number of samples. More details on this can be found in the book by Tsoulfanidis and Landsberger.[36]

In general, the quality of RPT results depends on system characteristics (size, uniformity, type, etc.) as well as RPT setup characteristics (number of detectors, arrangement of the detectors, etc.). Therefore, for comparison purposes, single tracer RPT tests were also carried out individually for tracers A and B in the same system. The averaged accuracy (p) and precision (σ) for these tracers are $p_A = 0.7$ mm, $\sigma_A = 1.3$ mm, $p_B = 0.8$ mm, and $\sigma_B = 1.6$ mm, respectively. In both cases, there is scattering in the calculated tracer positions and the corresponding standard deviations σ_A and σ_B are greater than the discrepancies p_A and p_B. This scattering comes from the fluctuations in emitted gamma rays due to the random nature of the radioactive decay. The standard deviation of these fluctuations is in fact equal to the square root of their mean values.[36] In fact, the slightly better precision of the results for tracer A (greater activity) can be explained by comparing the relative standard deviations of the measured event counts for both tracers. Although the raw event counts were passed through a Butterworth filter in the location algorithm, the filtered event counts still exhibit some fluctuations. Another source of scattering is the nonisotropic emission of gamma rays.

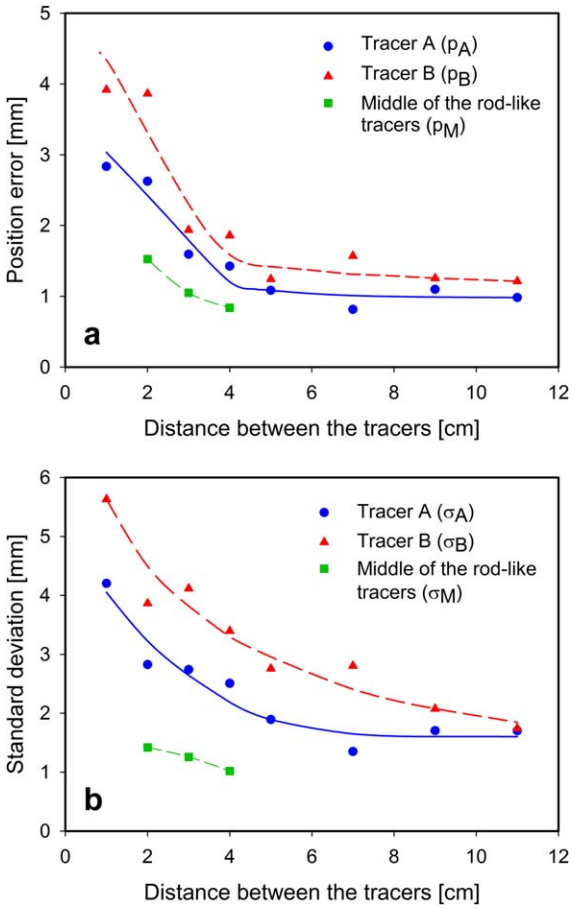

Figure 3. Variation of the (a) position error (accuracy) and (b) standard deviation (precision) of the position, as a function of the distance between the tracers.

[Color figure can be viewed in the online issue, which is available at wileyonlinelibrary.com.]

Stationary particle tests for the free MRPT technique

Using a 10-ms sampling time and a 12-s experiment duration, 1200 measurements were recorded for each stationary particle test. The filtered data start at zero and then level off to a slightly oscillating value after a certain time, which depends on how the filter parameters were chosen. Therefore, the first 600 tracer positions were rejected to eliminate physically meaningless information.

The variation in the position error and standard deviation vs. the distance between the tracers is displayed in Figure 3. It can be noticed that the accuracy and precision of the MRPT results are not as good as (larger values) than those of the RPT results ($p_A = 0.7$ mm, $\sigma_A = 1.3$ mm, $p_B = 0.8$ mm, and $\sigma_B = 1.6$ mm). In MRPT, the fluctuations in the gamma rays emitted by both tracers add up, leading to a larger standard deviation of the measured event counts. To calculate the relative standard deviation for each tracer in MRPT, the total standard deviation is divided by the mean

value of the event counts of each tracer individually ($\sigma_{rA}=\frac{\sigma_{(A,B)}}{\Phi_A}$ and $\sigma_{rB}=\frac{\sigma_{(A,B)}}{\Phi_B}$). Therefore, the relative standard deviation for each tracer is higher compared to that of RPT ($\sigma_{rA}=\frac{\sigma_A}{\Phi_A}$ and $\sigma_{rB}=\frac{\sigma_B}{\Phi_B}$), resulting in lower precision. The other reason for the lower precision of MRPT is due to the fact that the gamma rays emitted come from two tracers. In some cases, the calculated position for tracer A may be such that this tracer is closer than reality to some detectors. For these detectors (set #1), the contributions of tracer A to the total calculated event counts will be larger than what it should be, and those (set #2) related to the detectors that are further than expected will be smaller. Consequently, the contributions of tracer B associated with the set #1 of the detectors will be smaller and those related to set #2 will be larger. This means that the calculated position of tracer B is closer than reality to the detectors of set #2 and further to those of set #1. In other words, the positioning error related to tracer A will increase the positioning error of tracer B.

Figure 3 also shows that tracer A has better accuracy and precision than tracer B. Because of its lower activity, tracer B yields fewer event counts. Its relative standard deviation σ_{rB} is also larger, resulting in a lower precision compared to tracer A. It can be seen that the error and standard deviation decrease when the distance between the tracers increases. For a detector, the higher the contribution of tracer A (resp. B) in the measured event counts (the lower the relative standard deviation), the more effective it is in positioning tracer A (resp. B). When tracers A and B are far from each other, some of the detectors (set #1) are closer to tracer A and some other detectors (set #2) are closer to tracer B. The detectors of set #1 are then effective in the positioning of tracer A for two reasons: first, the contribution of tracer A in the total event counts is high and second, the impact on the standard deviation of the total event counts due to tracer B is small. Therefore, the relative standard deviation of tracer A is close to that of RPT for the detectors of set #1 under the same conditions. For similar reasons, the set #2 of detectors is then effective in the positioning of tracer B. When tracers A and B get close to each other, the detectors of set #1 and set #2 become similar. Therefore, in comparison with the previous case, the relative contribution of tracer A to the total event counts for the set #1 of detectors is smaller and the impact on the standard deviation of the total event counts due to tracer B is higher. Therefore, the relative standard deviation of tracer A is higher compared to that of the previous case, which means that the positioning of this tracer is not as good. Similar discussion can be done for tracer B.

Stationary particle tests for the restricted MRPT technique

In the restricted stationary MRPT tests, the middle point of the rod-like tracer is calculated by averaging the positions obtained for sources A and B with the standard approach. The accuracy and precision of the middle points for the three different rod-like tracers are illustrated in Figures 3. These results show a better accuracy and precision of the middle point positions than those of the individual sources. In some cases, the position of one of the sources is closer than reality to a group of detectors because of the fluctuations and nonisotropic emission of gamma rays. When this occurs, the corresponding group of detectors locates the other source at a larger distance to them to be compliant with the total event counts measured. This is why the middle point can be positioned more accurately than its two surrounding sources.

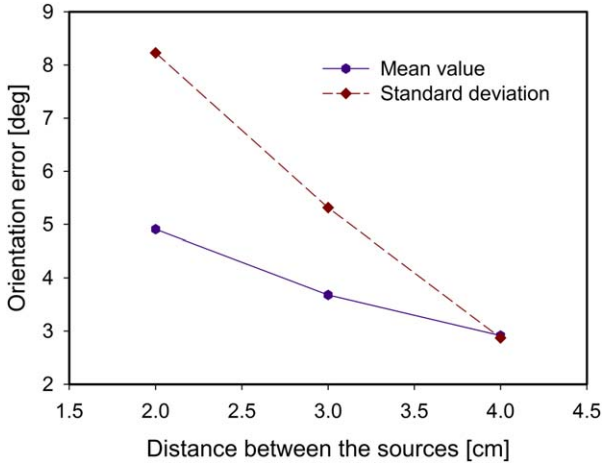

Figure 4. Variation of the mean error (accuracy) and standard deviation (precision) of the orientation of the rod-like tracers.

[Color figure can be viewed in the online issue, which is available at wileyonlinelibrary.com.]

One can take advantage of the fact that the middle points can be positioned more accurately and that the distance between the two tracers is known to determine their location more efficiently. Indeed, a rod-like tracer can be defined by its middle point position and the orientation vector connecting its two end points. The mean error and standard deviation of the orientation are depicted in Figure 4. It shows that the accuracy and precision increase with the distance between the sources. As the position error and standard deviation are higher at smaller distances (Figure 3), so is the orientation error. In addition, the larger the rod, the smaller the impact of a given position error on the orientation error will be.

To assess the ability of this alternative approach for positioning a rod-like tracer in restricted MRPT, the positions of the two sources located at the tips of a rod-like tracer were reconstructed from its length and the measured values of its middle point position and orientation. The mean error and standard deviation of the results obtained with this approach are illustrated in Figure 5. It can be readily noticed that the accuracy and precision are better for all three cases, and that the improvement is more important for the 2-cm long rod-like tracer. Note that the restricted MRPT results subsequently presented were obtained with this alternative approach.

Moving particle tests for the free MRPT technique

In the free MRPT moving particle tests, the tracers were set in motion independently along circles of radii 2, 3, 4, and 5 cm (see Figure 6). The tracer speed was varied from 22 to 56 mm/s for the different runs. Figure 6a shows the average positions of tracers A and B rotating along circles of 5 and 4 cm radii ($s_A = 56$ mm/s and $s_B = 46$ mm/s), respectively. Figure 6b shows typical average velocity vectors for the tracers in an *xy* plane for these runs. The results obtained indicate that the proposed MRPT technique can adequately measure the positions and speeds of the two tracers.

The results of the variation in the average position standard deviation and speed error vs. the speed of the tracers are

displayed in Figure 7. This figure shows an adequate resolution for these tracking experiments. As already discussed, tracer A can be located more precisely than tracer B. In these free MRPT tests, as the minimum distance between the tracers is more than 4 cm, the effect of the distance between the tracers on the results is expected to be very small (see Figure 3). Figure 7 shows that the position standard deviation and speed error are mainly dominated by the corresponding contribution in the z direction. Previous work from the literature[12,33] indicates that the results could be improved by placing the detectors on more than two levels along the z direction. In these moving particle tests, the fact that the tracers move during a recording interval causes an additional source of error compared to the stationary particle tests. This explains the small increase in the standard deviation of the tracer positions with respect to the speed of the tracers in the xy plane. Considering that the sampling time was 10 ms and the highest tracer speed was 56 mm/s, the tracers could then move a maximum of 0.56 mm during a recording interval. As this maximum displacement is much smaller than the MRPT resolution (see Figure 3), the accuracy of the results (position and speed error) is not significantly affected by the variation of the tracer speed within the range of speeds considered.

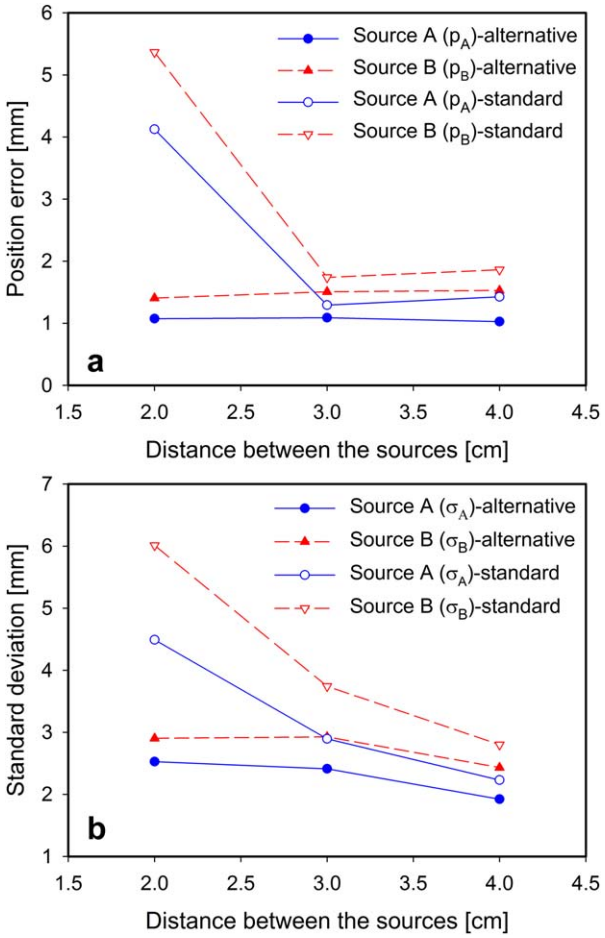

Figure 5. Comparison of the (a) accuracy and (b) precision obtained with the standard and alternative techniques for the restricted MRPT stationary tests.

[Color figure can be viewed in the online issue, which is available at wileyonlinelibrary.com.]

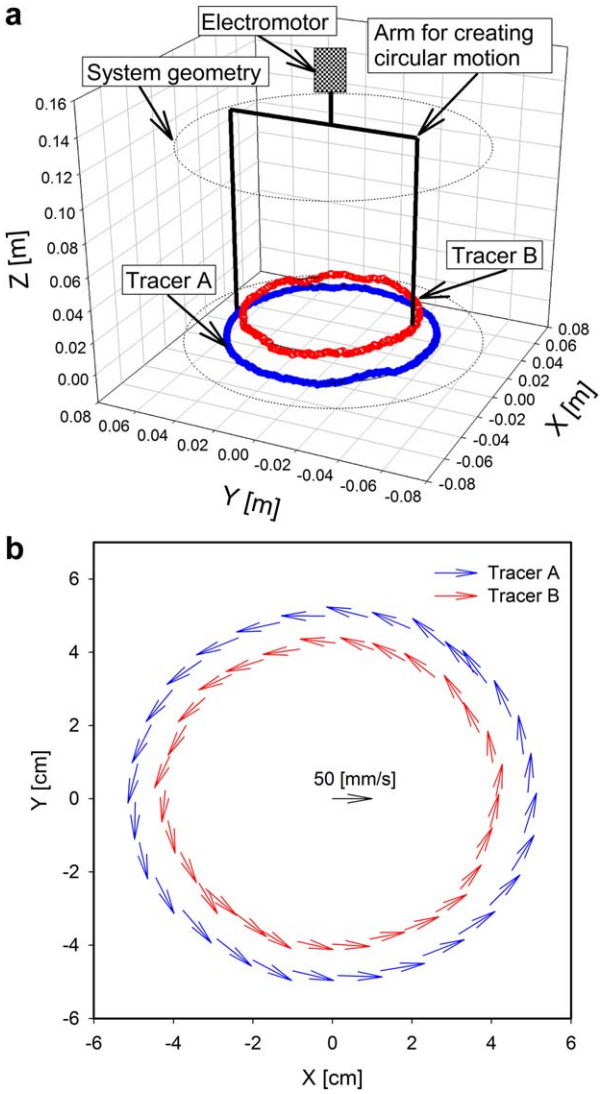

Figure 6. Tracers A and B rotating along 5- and 4-cm radius circles, respectively: (a) average position and (b) velocity vector.

[Color figure can be viewed in the online issue, which is available at wileyonlinelibrary.com.]

Moving particle tests for the restricted MRPT technique

In the restricted MRPT moving particle tests, the rod-like tracers were set in motion in a coupled manner along circles. The variation of the average position standard deviation and speed error corresponding to the middle point vs. the speed of the tracers is given in Figure 8. As already discussed, the resolution for rod-like tracers improves when the distance between the sources increase. This explains the trend observed in the figure. As the displacement of a tracer during a recording interval increases with its speed, so does its position standard deviation (Figure 8a). Because the electromotor has a constant rotational speed, the length of the arm was varied to adjust the speed of the tracers. Therefore, the tracers are closer to the wall of the system when their speed is higher, resulting in the decrease of the number of effective detectors and consequently, in the increase of the speed error and the position standard deviation (Figure 8). Despite it all, the resolution remains better than that of free MRPT (see Figure 7).

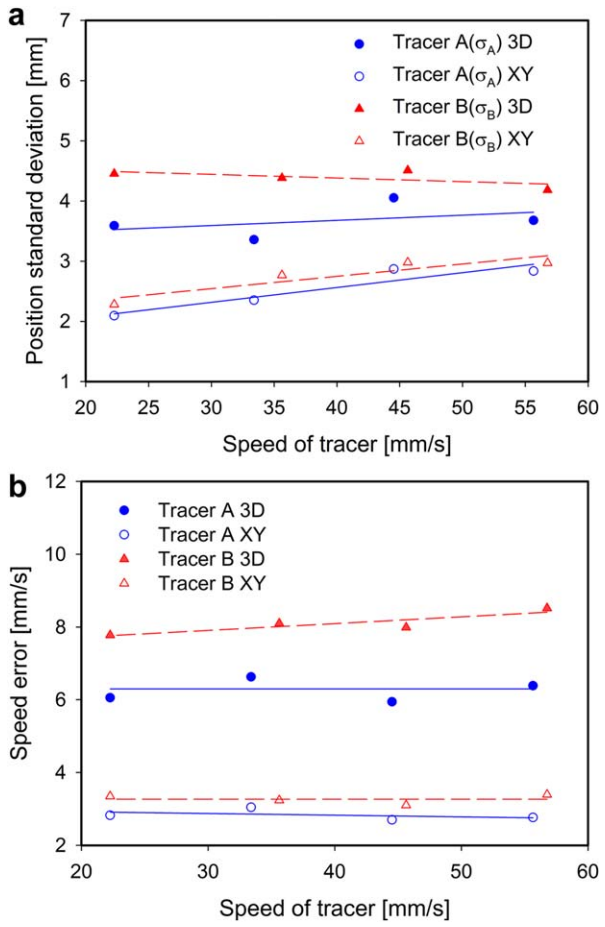

Figure 7. Variation of (a) the average position standard deviation and (b) the average speed error vs. the speed of the tracer in the free MRPT tests.

XY **means that only the contribution in the** x **and** y **directions were taken into account in the calculations of the corresponding quantities, whereas 3D means that all three directions were considered in these calculations. [Color figure can be viewed in the online issue, which is available at wileyonlinelibrary.com.]**

The variation of the mean error and standard deviation of the orientation of the rod-like tracers vs. the speed of these tracers is displayed in Figure 9. It can be noticed that the error is lower for the longer rods due to the larger distance between the sources. More precisely, it can be deduced that the orientation error and standard deviation are mainly dominated by the corresponding contributions in the z direction. The values of these quantities in the xy plane are similar to those for the stationary particle tests (Figure 4).

Flow in the rotating drum

To demonstrate the applicability of the proposed MRPT technique to investigate the flow dynamics in a realistic application, experiments were conducted in a rotating drum (2.5 rpm) filled with acrylic cylindrical particles 6 mm in diameter and 3 cm in length, mixed with 3-mm spherical glass beads, for a duration of 30 min. A rod-like tracer 3 cm in length was used to mimic the motion of the cylindrical particles based on the so-called ergodicity assumption (the time average of one tracer is equal to a population average[24]). At 2.5 rpm, the speed of the rod-like tracer could reach up to 25 cm/s (at the middle of free surface). There are two reasons for mixing cylindrical particles with glass beads. First, there are many applications where large particles are mixed with smaller particles: blending, transport, pyrolysis, sintering, drying, incineration, combustion. Second, such a test case gives us the possibility to assess qualitatively the MRPT results by visual observation. Because of the segregation mechanism between large and small particles, the cylindrical particles will migrate to the wall of the drum and the glass beads will settle near the middle of it.[26]

The speed of the tracer was calculated as the time derivative of its position. It is important to remember that the rod-like tracer position is defined by its middle point position. As the MRPT technique tracks a tracer in a Lagrangian manner, the domain was discretized into cells and the data were converted into Eulerian data. To obtain a velocity profile in a xy transverse plane, the tracer speeds in each cell were averaged regardless of the tracer position along the z axis.

Figure 10a shows the velocity profile of the cylindrical particles in the transverse plane. To eliminate the errors coming from the fluctuations in the tracer position and instantaneous speed, a large number of data is required for

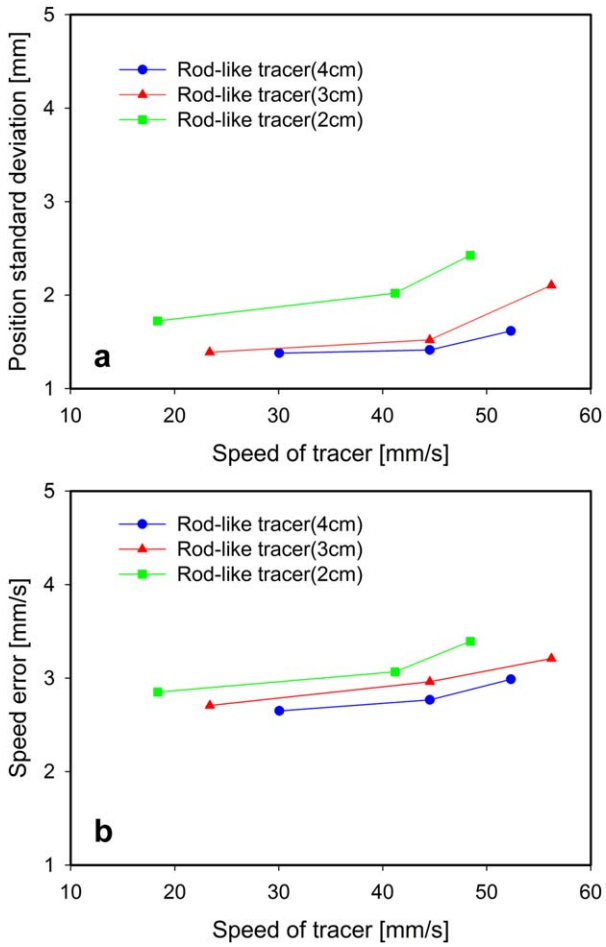

Figure 8. Variation in (a) the average position standard deviation and (b) the average speed error vs. the speed of the rod-like tracers in the restricted MRPT tests.

[Color figure can be viewed in the online issue, which is available at wileyonlinelibrary.com.]

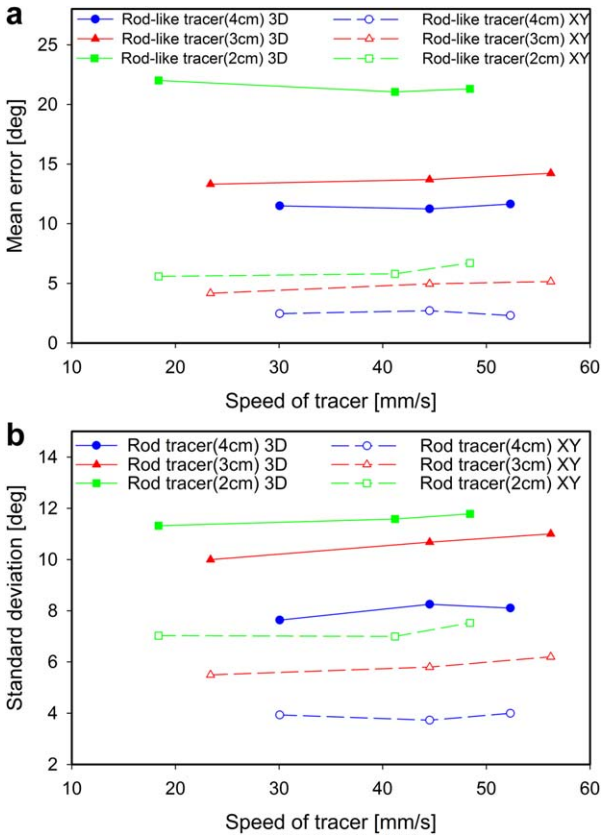

Figure 9. Variation of (a) the mean error and (b) the standard deviation of the orientation of the rod-like tracers vs. the speed of these tracers in the restricted MRPT tests.

***XY* means that only the contribution in the *x* and *y* directions were taken into account in the calculation of the corresponding quantities, whereas 3-D means that all three directions were considered in these calculations. [Color figure can be viewed in the online issue, which is available at wileyonlinelibrary.com.]**

each cell. An average of about 200 data points per cell were available to calculate the velocity profile, which is qualitatively in good agreement with that of spherical particles[26] (Figure 10b), except in regions where the free surface reaches the wall of the drum. It was observed that collisions between high-speed and low-speed particles occurring in the low extremity of the free surface often resulted in the jump of a few cylindrical particles. Such collisions also generated a disorder of these particles in this section of the bed. Figure 10a also indicates that the rod-like tracer could not reach the core of the bed owing to segregation between the spherical and cylindrical particles.

Figure 11a shows the position and orientation of the rod-like tracer during a single circulation of the tracer. To visualize in an effective manner the orientation of cylindrical particles during the circulation, the L axis is introduced and defined as the axis that passes through the center of the domain and is parallel to the free surface, while the angle θ is defined as the angle between the rod-like tracer and this L axis. We recall that the motion of the particles in a rotation drum is generally investigated by dividing the bed into two sections: (1) a thin lens-like layer beneath the free surface called active layer wherein the particles slide downward and (2) a large passive layer underneath the active layer where the particles flow along arcs of different radii. Figure 11b shows average values of θ in both sections. It can be observed that when the particles reach the free surface (top left part in Figure 11a), their orientation angles are wide. When sliding along the free surface, these angles decrease until the particles reach around $L = -8$ cm. Downstream from this region, the particles slide almost parallel to the free surface ($\theta = 0$) until they reach around $L = 6$ cm, after which their orientation angles start increasing until they hit the wall of the drum. One can also notice in Figure 11 that particles located on the free surface near $L = 10$ cm can have wide orientation angles, which enable them to penetrate more easily into the passive layer of the bed. These particles then flow in a solid-like body motion, as evidenced by the constant decrease rate of their orientation angles (Figure 11b).

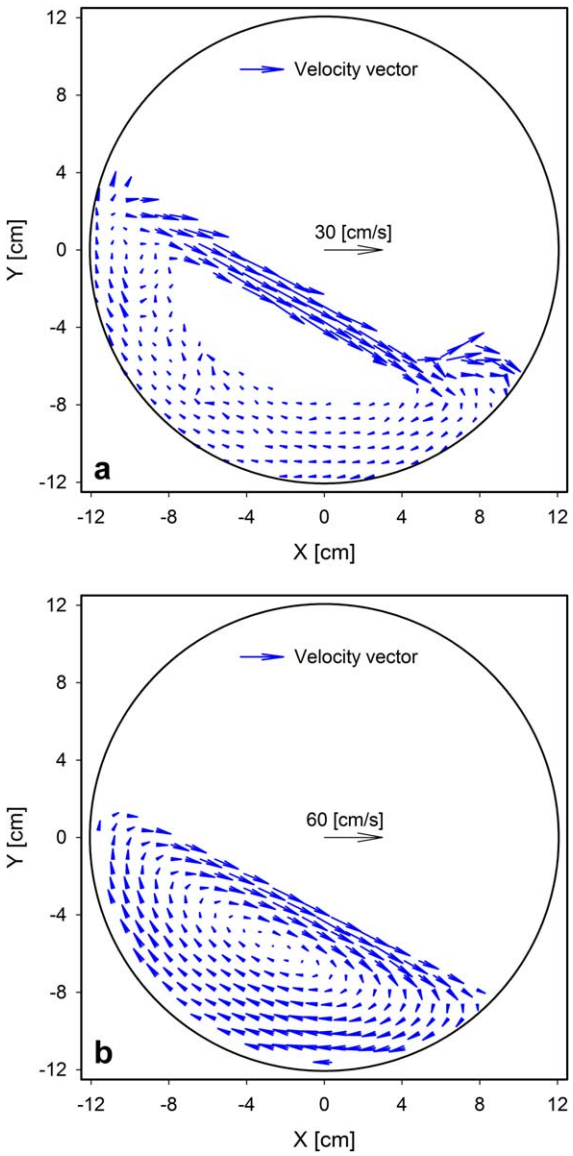

Figure 10. Velocity vectors in the transverse plane of the drum for (a) cylindrical particles after 30 min and a rotational speed of 2.5 rpm, (b) 3-mm glass beads and a rotational speed of 11.6 rpm (this figure is adapted from Ref. 26, with permission from Wiley).

[Color figure can be viewed in the online issue, which is available at wileyonlinelibrary.com.]

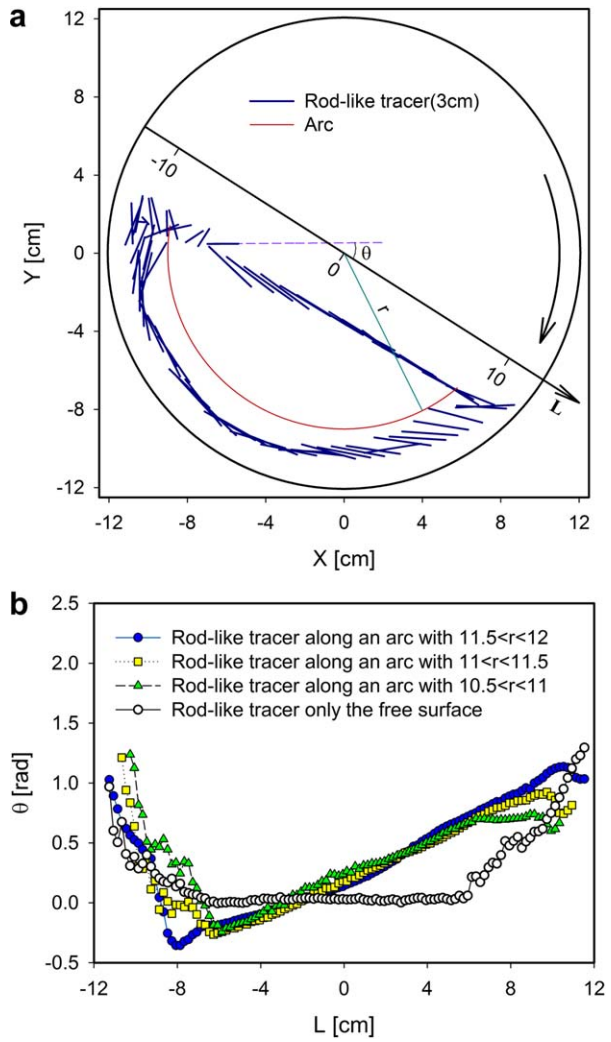

Figure 11. (a) Rod-like tracer position and orientation during a single circulation and (b) average angle of this tracer along the *L* axis during the circulations.

[Color figure can be viewed in the online issue, which is available at wileyonlinelibrary.com.]

Alternatively, these particles may remain in the active layer for a while before entering the passive layer. What one should appreciate here is that such information could not be provided by single tracer RPT.

Conclusion

This work shows that the proposed MRPT technique can simultaneously track two tracers that move freely or are at a fixed distance from each other. By conducting stationary and moving particle tests, it was demonstrated that MRPT can position two tracers with an error similar to that with single tracer RPT when the distance between these tracers is more than 4 cm. It was also observed that when the distance between the two tracers is fixed, the middle point (<2 mm) and orientation of the tracers (<5°) can be measured adequately with this technique. Finally, the MRPT technique was applied to the flow of spherical and cylindrical particles (3 cm in length, speed up to 25 cm/s) in a cylindrical drum (2.5 rpm). Good results were obtained as regards the position and orientation of the cylindrical particles using a rod-like tracer to mimic the motion of these cylindrical particles.

Future work will include the impact of the activity ratio between two tracers comprising a nonspherical particle on the efficiency of the MRPT technique, particularly when the distance between these two tracers is small.

Acknowledgments

The authors acknowledge the financial support from Praxair and the Natural Sciences and Engineering Research Council of Canada. The authors are grateful to Cornelia Chilian from the Institute of Nuclear Engineering for the activation of tracers, Dr. Greg Kennedy for his helpful discussion about the MRPT technique with different isotopes, and Dr. Ebrahim Alizadeh for his help with the computer codes used in this work and for providing the data points for Figure 10b.

Literature Cited

1. Chaouki J, Larachi F, Dudukovic MP. Noninvasive tomographic and velocimetric monitoring of multiphase flows. *Ind Eng Chem Res*. 1997;36(11):4476–4503.
2. Boyer C, Duquenne AM, Wild G. Measuring techniques in gas-liquid and gas-liquid-solid reactors. *Chem Eng Sci*. 2002;57(16):3185–3215.
3. Parker DJ, Broadbent CJ, Fowles P, Hawkesworth MR, McNeil P. Positron emission particle tracking-a technique for studying flow within engineering equipment. *Nucl Instrum Methods Phys Res Sect A*. 1993;326(3):592–607.
4. Bakalis S, Fryer PJ, Parker DJ. Measuring velocity distributions of viscous fluids using positron emission particle tracking (PEPT). *AIChE J*. 2004;50(7):1606–1613.
5. Guida A, Nienow AW, Barigou M. Mixing of dense binary suspensions: multi-component hydrodynamics and spatial phase distribution by PEPT. *AIChE J*. 2011;57(9):2302–2315.
6. Link JM, Deen NG, Kuipers JAM, Fan X, Ingram A, Parker DJ, Wood J, Seville JPK. PEPT and discrete particle simulation study of spout-fluid bed regimes. *AIChE J*. 2008;54(5):1189–1202.
7. Ng BH, Kwan CC, Ding YL, Ghadiri M, Fan XF, Parker DJ. Granular flow fields in vertical high shear mixer granulators. *AIChE J*. 2008;54(2):415–426.
8. Leadbeater TW, Parker DJ, Gargiuli J. Positron imaging systems for studying particulate, granular and multiphase flows. *Particuology*. 2012;10(2):146–153.
9. Doucet J, Bertrand F, Chaouki J. An extended radioactive particle tracking method for systems with irregular moving boundaries. *Powder Technol*. 2008;181(2):195–204.
10. Lin JS, Chen MM, Chao BT. A novel radioactive particle tracking facility for measurement of solids motion in gas fluidized beds. *AIChE J*. 1985;31(3):465–473.
11. Godfroy L, Larachi F, Kennedy G, Grandjean B, Chaouki J. On-line flow visualization in multiphase reactors using neural networks. *Appl Radiat Isot*. 1997;48(2):225–235.
12. Roy S, Larachi F, Al-Dahhan MH, Dudukovic MP. Optimal design of radioactive particle tracking experiments for flow mapping in opaque multiphase reactors. *Appl Radiat Isot*. 2002;56(3):485–503.
13. Chen JW, Rados N, Al-Dahhan MH, Dudukovic MP, Nguyen D, Parimi K. Particle motion in packed/ebullated beds by CT and CARPT. *AIChE J*. 2001;47(5):994–1004.
14. Larachi F, Cassanello M, Chaouki J, Guy C. Flow structure of the solids in a 3-D gas-liquid-solid fluidized bed. *AIChE J*. 1996;42(9):2439–2452.
15. Larachi F, Chaouki J, Kennedy G. 3-D mapping of solids flow-fields in multiphase reactors with RPT. *AIChE J*. 1995;41(2):439–443.
16. Roy S, Kernoun A, Al-Dahhan MH, Dudukovic MP. Experimental investigation of the hydrodynamics in a liquid-solid riser. *AIChE J*. 2005;51(3):802–835.
17. Mostoufi N, Chaouki J. Flow structure of the solids in gas-solid fluidized beds. *Chem Eng Sci*. 2004;59(20):4217–4227.
18. Degaleesan S, Dudukovic M, Pan Y. Experimental study of gas-induced liquid-flow structures in bubble columns. *AIChE J*. 2001;47(9):1913–1931.

19. Xu SK, Qu YH, Chaouki J, Guy C. Characterization of homogeneity of bubble flows in bubble columns using RPT and fibre optics. *Int J Chem React Eng*. 2005;3:1–14.
20. Guha D, Ramachandran PA, Dudukovic MP, Derksen JJ. Evaluation of large eddy simulation and Euler-Euler CFD models for solids flow dynamics in a stirred tank reactor. *AIChE J*. 2008;54(3):766–778.
21. Guha D, Ramachandran PA, Dudukovic MP. Flow field of suspended solids in a stirred tank reactor by Lagrangian tracking. *Chem Eng Sci*. 2007;62(22):6143–6154.
22. Larachi F, Grandjean BPA, Chaouki J. Mixing and circulation of solids in spouted beds: particle tracking and Monte Carlo emulation of the gross flow pattern. *Chem Eng Sci*. 2003;58(8):1497–1507.
23. Cassanello M, Larachi F, Legros R, Chaouki J. Solids dynamics from experimental trajectory time-series of a single particle motion in gas-spouted beds. *Chem Eng Sci*. 1999;54(13–14):2545–2554.
24. Doucet J, Bertrand F, Chaouki J. Experimental characterization of the chaotic dynamics of cohesionless particles: application to a V-blender. *Granular Matter*. 2008;10(2):133–138.
25. Sherritt RG, Chaouki J, Mehrotra AK, Behie LA. Axial dispersion in the three-dimensional mixing of particles in a rotating drum reactor. *Chem Eng Sci*. 2003;58(2):401–415.
26. Alizadeh E, Dube O, Bertrand F, Chaouki J. Characterization of mixing and size segregation in a rotating drum by a particle tracking method. *AIChE J*. 2013;59(6):1894–1905.
27. Dube O, Alizadeh E, Chaouki J, Bertrand F. Dynamics of non-spherical particles in a rotating drum. *Chem Eng Sci*. 2013;101:486–502.
28. Mostoufi N, Kennedy G, Chaouki J. Decreasing the sampling time interval in radioactive particle tracking. *Can J Chem Eng*. 2003;81(1):129–133.
29. Duchanoy C, Jongen TRG. Efficient simulation of liquid-solid flows with high solids fraction in complex geometries. *Comput Fluids*. 2003;32(10):1453–1471.
30. Mankad S, Fryer PJ. A heterogeneous flow model for the effect of slip and flow velocities on food steriliser design. *Chem Eng Sci*. 1997;52(12):1835–1843.
31. Yang Z, Fan X, Bakalis S, Parker DJ, Fryer PJ. A method for characterising solids translational and rotational motions using multiple-positron emission particle tracking (multiple-PEPT). *Int J Multiphase Flow*. 2008;34(12):1152–1160.
32. Beam GB, Wielopolski L, Gardner RP, Verghese K. Monte Carlo calculation of efficiencies of right-circular cylindrical NaI detectors for arbitrarily located point sources. *Nucl Instrum Methods*. 1978;154(3):501–508.
33. Larachi F, Kennedy G, Chaouki J. A gamma-ray detection system for 3-D particle tracking in multiphase reactors. *Nucl Instrum Methods Phys Res Sect A*. 1994;338(2–3):568–576.
34. Knoll GF. *Radiation Detection and Measurement*. USA: Wiley, 2010.
35. Chaouki J, Larachi F, Dudukovic P. *Non-Invasive Monitoring of Multiphase Flows*. The Netherlands: Elsevier Science, 1997.
36. Tsoulfanidis N, Landsberger S. *Measurement and Detection of Radiation*. USA: CRC Press, 2011.
37. Dube O, Chaouki J, Bertrand F. Optimization of detector positioning in the radioactive particle tracking technique. *Appl Radiat Isot*. 2014;89:109–124.

APPENDIX

In this appendix, the noise coming from the tracer with higher energy peak (tracer B) on the event counts of the other tracer (tracer A) is calculated. To do so, a Monte Carlo approach is considered. In the rotating drum, 200 pair positions for tracers A and B are chosen randomly (Figure A1a). For a given pair of positions, to calculate the amount of gamma rays that are scattered from tracer B, two different situations are considered: first, with an empty drum and next, with a drum filled with particles. The difference between the event counts for these two situations is related to the amount of scattered gamma rays. Only a portion of these scattered gamma rays will end up in the energy window of tracer A. Here, it is assumed that this portion is 20%. Therefore, the event counts of tracer A, the noise from tracer B on the event counts of tracer A, and the noise to signal ratio for tracer A can be calculated (Figure A1b). To ease the analysis, only 100 data points are displayed in Figure A1b. It shows that the noise to signal ratio varies significantly with the pair position of tracers A and B. While in some cases the noise is negligible, in many cases it can be large. The averaged noise to signal ratio is about 0.6 (calculated from the 200 data points), which is very high and likely to result in poor positioning of tracer A.

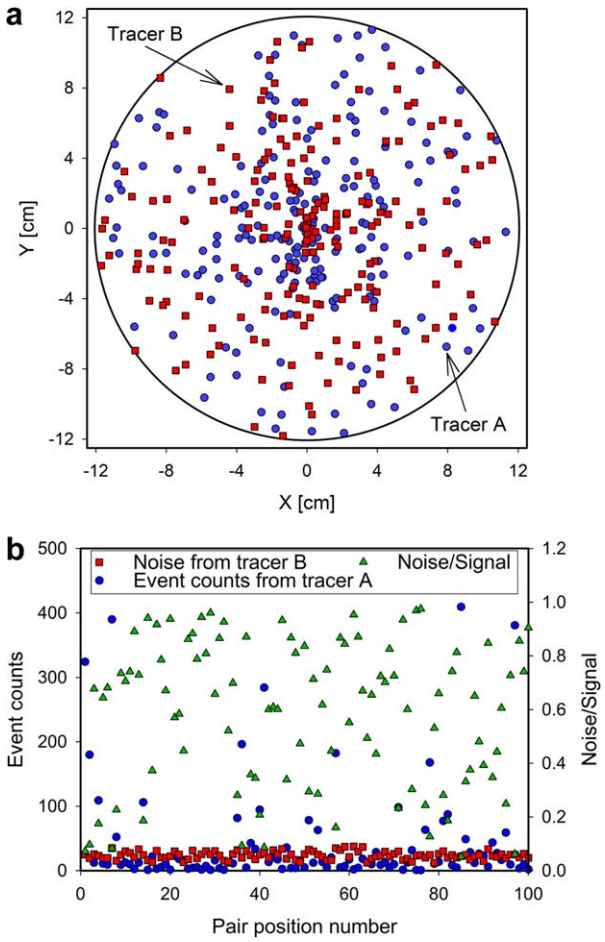

Figure A1. (a) Distribution of pair positions for tracers A (blue) and B (red) in the drum and (b) event counts for tracer A, the noise from tracer B on the event counts of tracer A, and the noise to signal ratio for tracer A, for each pair position.

[Color figure can be viewed in the online issue, which is available at wileyonlinelibrary.com.]

Manuscript received May 30, 2014, and revision received Sep. 19, 2014.